Eigenmodes of the dynamically coupled twin-stripe semiconductor laser

Ortwin Hess and Eckehard Schöll

Institut für Theoretische Physik, Technische Universität Berlin, D - 10623 Berlin, Germany
(Received 29 November 1993)

The twin- stripe semiconductor laser is analyzed theoretically through the nonlinear eigenmodes of the spatiotemporal distribution of the output intensity. The transverse laser modes in three spatiotemporal regimes are identified as a function of stripe separation: the regime of quasi-isolated independently operating laser stripes leading to a continuous-wave output, the intermediate regime with the laser displaying chaotically pulsating signals, and the strong-coupling regime with high-frequency more regular oscillations due to a reduced number of active spatiotemporal degrees of freedom.

PACS number(s): 42.50.Ne, 42.55.Px, 05.45.+b

Semiconductor laser arrays are spatially distributed nonlinear model systems which display complex spatiotemporal dynamics. In the twin-stripe semiconductor laser, two laser stripes, each by itself representing a nonlinear oscillator, are combined in one single device. Transversely overlapping evanescent optical fields and diffusion of charge carriers — which are injected through contact stripes on the top of the laser device (cf. Fig. 1) — provide the physical mechanisms for the mutual interaction between the two laser oscillators. The dynamics of the twin-stripe laser is strongly influenced by the transverse coupling between the two laser stripes. Frequently, the highly nonlinear processes in and between them lead to the spontaneous, i.e., self-organized, formation of regular or turbulent structures in the output signal [1]. Arrays of coupled lasers and the resulting chaotic dynamics have been modeled by discrete coupled nonlinear oscillators [2,3], involving ordinary differential equations. The spatial average of the output signal can often be adequately described by such coupled mode approaches [4]. However, the full spatiotemporal dynamics and its dependence upon the stripe geometry can only be understood in terms of continuous-space models, i.e., partial differential equations as used in this work. The spatiotemporal patterns found in our numerical simulations of the output intensity are strikingly complex and the underlying dynamics is hard to grasp by visual in-

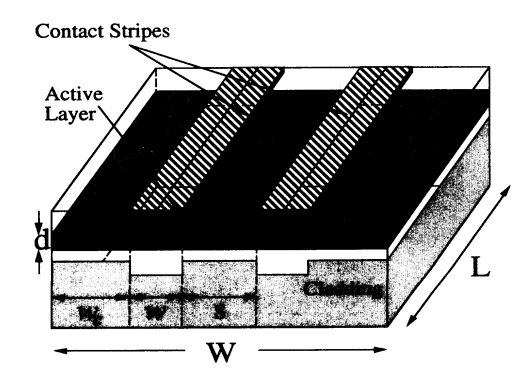


FIG. 1. Schematic structure of a combined gain- and indexguided GaAs/Al_xGa_{1-x}As twin-stripe laser.

spection. Our main issue is to demonstrate a systematic procedure to extract the generic eigenmodes, rather than approximate the spatial dimension in the spatiotemporal intensity distribution of the laser by projection onto a "guessed" set of transverse optical modes (e.g., Gauss-Hermite modes). By calculating the set of these particular eigenmodes we identify the relevant nonlinear spatial patterns and their temporal evolution, e.g., the broken spatial symmetry and the temporal and spatial variation of the coupling between the two laser stripes. With the laser as a model system, we demonstrate the usefulness of this eigenmode analysis for the characterization of spatiotemporal complexity in a much wider class of spatially distributed nonlinear systems.

The dynamics of the longitudinally (in z direction, cf. Fig. 1) slowly varying counterpropagating optical fields E^{\pm} and the dynamics of the electron-hole density N are described by the following model system of coupled nonlinear partial differential equations [5,6]

$$\begin{split} \pm \frac{\partial E^{\pm}}{\partial z} + \frac{n_l}{c} \frac{\partial E^{\pm}}{\partial t} &= iD_p \frac{\partial^2 E^{\pm}}{\partial x^2} - i\kappa(x)E^{\pm} \\ &\quad + \Gamma(x) \left[g(N) - i\alpha aN \right] E^{\pm}, \qquad (1) \\ \frac{\partial N}{\partial t} &= \Lambda(x) + D_f \frac{\partial^2 N}{\partial x^2} - \frac{N}{\tau} \\ &\quad - g(N) \left(|E^+|^2 + |E^-|^2 \right). \quad (2) \end{split}$$

The optical gain and the change of the refractive index of the active medium are modeled by $g(N)=a(N-N_0)$ and $\delta n=-\alpha aN/k_0$, respectively [7], where the differential gain is $a=1.5\times 10^{-16}~{\rm cm}^2$, $N_0=0.64\times 10^{18}~{\rm cm}^{-3}$ is the carrier density at transparency, $n_l=3.59$ is the refractive index of the active semiconductor layer, $k_0=2\pi/\lambda$ is the wave number in vacuum, $\lambda=815~{\rm nm}$ the optical wavelength, c the speed of light, and ε_0 is the vacuum permittivity. The linewidth enhancement factor $\alpha=2$ is assumed constant. The nonradiative decay of the electron-hole density is represented by the relaxation time $\tau=5~{\rm ns}$. The diffraction coefficient $D_p=(2n_lk_0)^{-1}=18\times 10^{-6}~{\rm m}$ results from the paraxial ray approximation [8] which has been performed to obtain (1) from Maxwell's equations [5]. The transverse passive waveguiding properties are characterized by $\kappa(x)=k_0~(n_c-n_{\rm eff})$ for $x_i-w/2\leq x\leq x_i+w/2$ and

 $\kappa(x) = k_0 n_c$ in the regions between the stripes, where x_i , i = 1, 2 is the center of the *i*th laser, $w = 5 \mu \text{m}$ its width, $n_{\text{eff}} = 3.42$ its effective index, and $n_c = 3.35$ is the refractive index of the cladding layer. The confinement factor $\Gamma(x) = 0.5149$ for $x_i - w/2 \le x \le x_i + w/2$ and $\Gamma(x) = 0.5013$ between the laser stripes, represents the transverse dependence of the vertical confinement of the optical field to the active layer. The reflection of the optical fields at the facet mirrors at z = 0 and $z = L = 250 \mu m$ of the laser structure is described by the longitudinal boundary conditions $E^+(x,0,t) =$ $-\sqrt{R_1}E^-(x,0,t), E^-(x,L,t) = -\sqrt{R_2}E^+(x,L,t), \text{ with }$ $R_1 = 0.32$ and $R_2 = 0.99$. The transverse boundary conditions $\partial E^{\pm}/\partial x = -\alpha_w E^{\pm}, \partial N/\partial x = -\alpha_{\rm sr} N$ at x = +W/2 and $\partial E^{\pm}/\partial x = +\alpha_w E^{\pm}, \partial N/\partial x = +\alpha_{\rm sr}N$, x = -W/2, where $W = s + 2w + 2w_c$, with s being the stripe separation, account for the absorption $(\alpha_w = 30 \text{ cm}^{-1})$ in the "wings" $(w_c = 10 \mu\text{m})$ outside the laser stripes, and the charge carrier recombination effects at the surface of the structure. The surfacerecombination coefficient [9] $\alpha_{\rm sr} = v_{\rm sr}/D_f$ includes the diffusion-coefficient $D_f = 30 \text{ cm}^2/\text{s}$ and the surface-recombination velocity $v_{\rm sr} = 10^6 \text{ m/s}$. The coupled system of nonlinear partial differential equations (1) and (2) is discretized in time (t) and space (x, z) and the resulting finite-difference equations are integrated using the Hopscotch method [6,10]. We have varied the interelement distance s between the two laser stripes, being the prominent coupling parameter between the two nonlinear laser oscillators, in the regime between 5 μ m and 16 μ m, while all further parameters remain unchanged. The

transversely dependent excitation of the two oscillators — determined by the injection of charge carriers through the two contact stripes (hatched in Fig. 1) at the top of the device — is applied at t=0 with a step function and held constant in time. It is represented by the pumping term $\Lambda(x)=j\eta/(ed)$ for $x_i-w/2\leq x\leq x_i+w/2$ and $\Lambda(x)=0$ otherwise. The injection current density is denoted by $j,\ \eta=0.5$ represents the injection efficiency, e is the electron charge and $d=0.15\ \mu\mathrm{m}$ the (vertical) thickness of the layer.

Figures 2 (a) - 4 (a) show the dynamics of the output intensity at the front facet $I(x,t) = T_1 \mid E^-(x,z) = T_1 \mid E^-(x,z) = T_1 \mid E^-(x,z) \mid E^-($ $|0,t|^2/Z$, $Z = n_l/(\varepsilon_0 c)$ and $T_1 = 1 - R_1$ being the optical wave resistance in the semiconductor medium and the transmittivity of the front mirror, respectively, during the time interval from $t_1 = 20$ ns to $t_2 = 25$ ns after the start of the laser. Three different dynamic regimes can be distinguished when the interelement coupling is varied from the weakly coupled case at a stripe separation $s \ge 14 \,\mu\mathrm{m}$ (Fig. 2), via the range of intermediate coupling (Fig. 3) to the strongly coupled case (Fig. 4) at $s = 5 \mu m$. In Fig. 2 (a) the two laser stripes operate independently in a stable continuous-wave (cw) mode. If s is decreased below $s = 14 \mu m$, a sharp, symmetry-breaking transition occurs to a time-dependent state where both laser stripes pulsate erratically [Fig. 3 (a)], showing apparently chaotic intensity spikes which are strikingly similar to previously reported streak-camera measurements [11]. Finally, at a stripe separation of $s = 5 \mu m$ [Fig. 4 (a)], the intensity shows high frequency more regular out-ofphase oscillations of the two laser stripes. This behavior

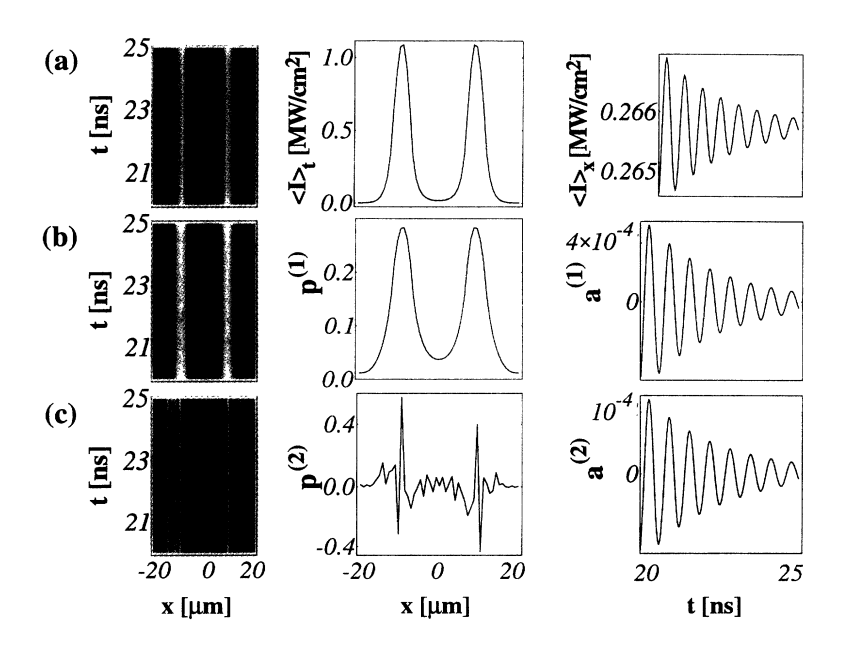


FIG. 2. Computed near-field intensity I(x,t) for the weakly coupled twin-stripe semiconductor laser at a stripe separation of $s=14~\mu\mathrm{m}$. (a) Original spatiotemporal intensity distribution (Bright colors represent high light intensity, dark shading indicates low intensity values); temporally averaged intensity $\langle I \rangle_t$; transverse spatial average $\langle I \rangle_x$. (b) Reconstructed spatiotemporal intensity distribution, eigenvector $\mathbf{p}^{(1)}$, and expansion coefficient $a^{(1)}$, obtained by projection onto the fundamental eigenmode $(\lambda^{(1)}=0.9983)$. (c) Projection onto the second eigenmode $(\lambda^{(2)}<10^{-3})$. The analysis is done for M=51. Only in the reconstructed intensity distribution of the first mode $\langle I \rangle_t$ has been added.

has been corroborated by computing much longer time series and different stripe separations. In order to identify the complex nonlinear interactions of the different spatiotemporal degrees of freedom and gain insight into the physical coupling mechanisms, we apply a singular spectrum analysis or Karhunen-Loève decomposition [12–14] to our computed data in the time interval $T=t_2-t_1$. To this purpose we calculate the spatial covariance matrix of the transversely discretized intensity distribution

$$C_{k,l} = \langle u(x_k, t)u(x_l, t)\rangle_t, \tag{3}$$

where k, l = 1, 2, ..., M number the discrete trans-

verse points x_k and $\langle \rangle_t$ denotes the temporal average $\int_{t_1}^{t_2} dt/T$. Here we have introduced the intensity fluctuation $u(x,t) \equiv \delta I(x,t)/\sqrt{\langle I(x,t)\rangle_t}$ with $\delta I(x,t) = I(x,t) - \langle I(x,t)\rangle_t$ normalized such that u^2 has the dimension of an optical intensity. The eigenvectors \mathbf{p} of C_{kl} then represent an optimal basis for expansion of I(x,t) in the sense that they maximize the projected mean $\langle (\mathbf{p},u)^2\rangle_t$, where $(\mathbf{p},u) = \sum_k \mathbf{p}(x_k)u(x_k,t)$ denotes the scalar product; i.e., for a given accuracy the minimum number of eigenvectors is needed in the expansion. By construction, $C_{k,l}$ is symmetric and its eigenvalues $\lambda^{(\alpha)}$ ($\alpha = 1, \ldots, M$, ordered according to

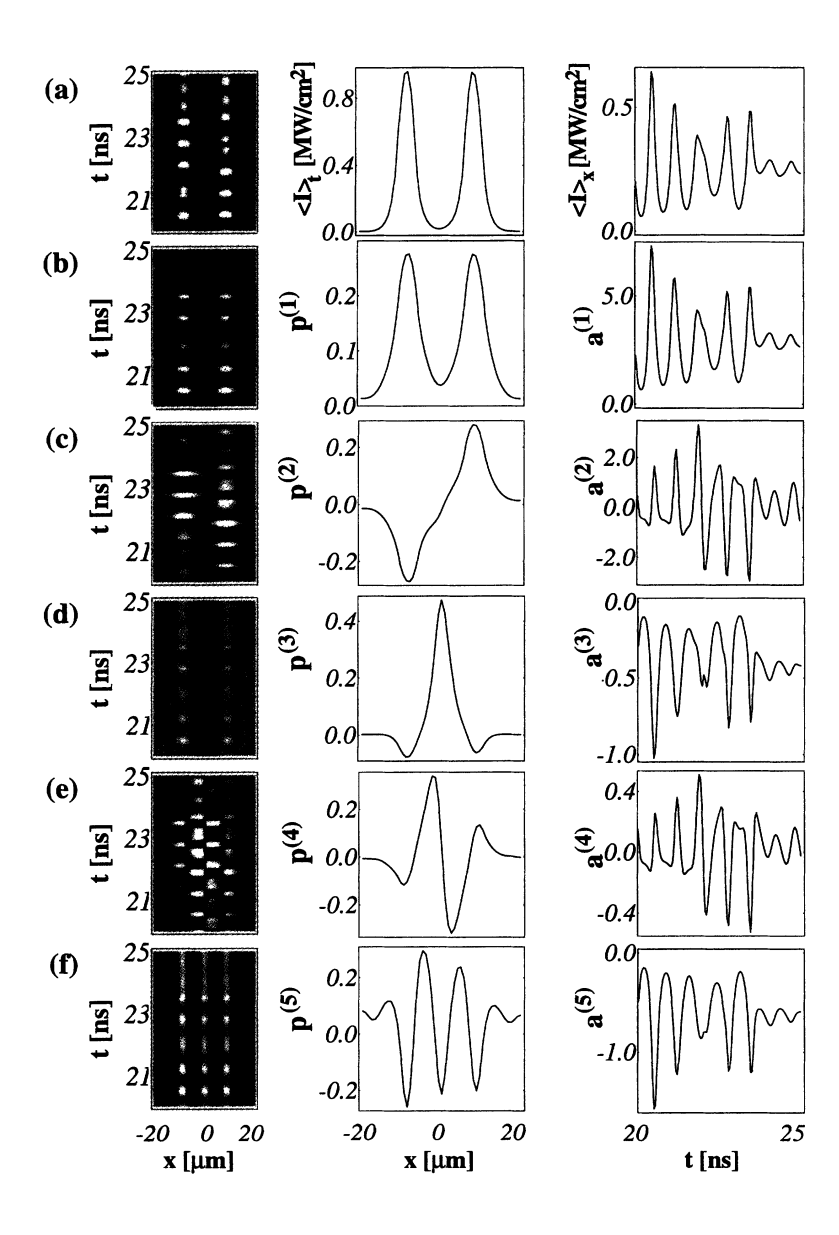


FIG. 3. Intermediate coupling regime (s = 12 μ m). (a) Original, (b) – (f) reconstructed spatiotemporal intensity distribution, obtained by projection onto the fundamental mode ($\lambda^{(1)}=0.5822$) (b), the symmetry-breaking mode ($\lambda^{(2)}=0.4001$) (c), the coupling mode ($\lambda^{(3)}=1.412\times10^{-2}$) (d), and the bimodal ($\lambda^{(4)}=2.935\times10^{-3}$) (e) and trimodal modes ($\lambda^{(5)}=1.58\times10^{-4}$) (f).

decreasing values) determine the probability of the occurrence of the corresponding eigenvectors \mathbf{p}^{α} in the intensity field u(x,t). In the following, the eigenvalues are normalized by $E \equiv \langle (u,u) \rangle_t = \sum_{\alpha=1}^M \lambda^{(\alpha)}$. The M eigenvectors $\mathbf{p}^{(\alpha)}(x_k)$ form a complete orthonormal set $\sum_k \mathbf{p}^{(\alpha)}(x_k) \mathbf{p}^{(\beta)}(x_k) = \delta^{\alpha\beta}$ and are used as basis functions for an expansion of the original intensity distribution

$$I(x_k, t) = \langle I(x_k, t) \rangle_t + \sum_{\alpha} a^{(\alpha)}(t) \mathbf{p}^{(\alpha)}(x_k), \tag{4}$$

with the expansion coefficients $a^{(\alpha)}(t) = \sum_{k} \mathbf{p}^{(\alpha)}(x_k) \, \delta I(x_k, t)$. In the weakly coupled case at $s = 14 \, \mu \text{m}$ where the twin-stripe laser shows a continuous-wave output signal [Fig. 2 (a)], the projec-

tion $\langle I(x_k,t)\rangle_t + a^{(1)}(t)\mathbf{p}^{(1)}(x_k)$ of the intensity onto the first eigenvector $\mathbf{p}^{(1)}$ [Fig. 2 (b)] very closely resembles the original intensity picture [Fig. 2 (a)]. Note the striking similarities between the time-averaged signal $\langle I \rangle_t = \int_{t_1}^{t_2} I(x,t) dt/T$ and the first eigenvector $\mathbf{p}^{(1)}$, as well as between $a^{(1)}(t)$ and $\langle I \rangle_x = \int_{-W/2}^{W/2} I(x,t) dx/W$. Not surprisingly, the first eigenvalue $\lambda^{(1)} = 0.9983$ is dominant. The following $\lambda^{(\alpha)}$ of order $\alpha \geq 2$ are rapidly decreasing. The corresponding eigenmodes $\mathbf{p}^{(\alpha)}$ and coefficients $a^{(\alpha)}(t)$ appear noisy and jagged [Fig. 2 (c)]. At the stripe separation $s = 12 \mu m$, however, there is a clear difference between the original spatiotemporal intensity distribution [Fig. 3(a)] and the projection of the intensity field onto the first eigenmode $p^{(1)}$ [Fig. 3(b)]. While in Fig. 3 (a) the intensity displays the onset of chaotic oscillations where the phase coherence between the left

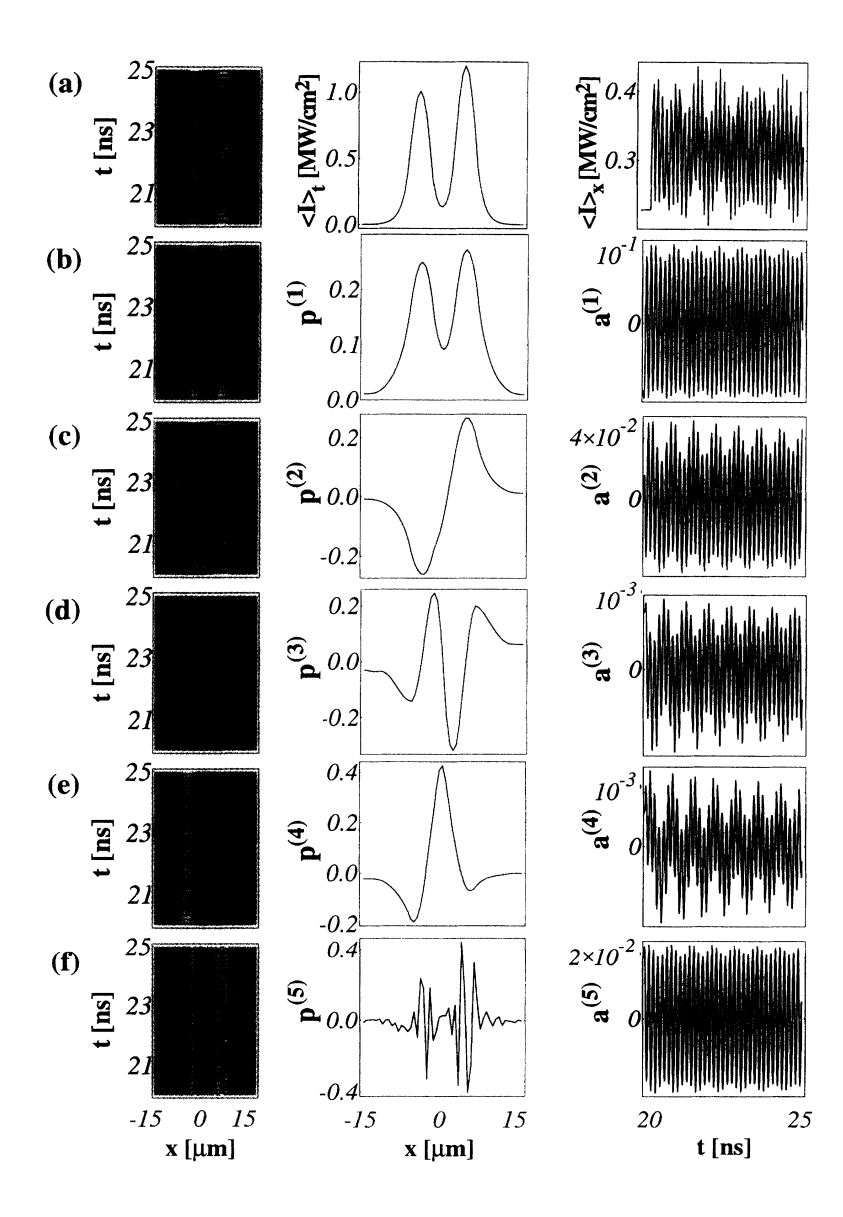


FIG. 4. Same as Fig. 3, but for the strong-coupling regime $(s=5~\mu\mathrm{m})$. (b) $\lambda^{(1)}=0.8534$, (c) $\lambda^{(2)}=0.1459$, (d) $\lambda^{(3)}=6.7\times10^{-4}$, (e) $\lambda^{(4)}=1.19\times10^{-6}$, (f) $\lambda^{(5)}=2.27\times10^{-7}$.

stripe and the right one is lost, the intensity projection in Fig. 3 (b) shows the two laser stripes oscillating synchronously. The fundamental mode describes synchronized pulsations which may still be chaotic [2]. Only the next contribution, the projection $a^{(2)}(t)\mathbf{p}^{(2)}(x_k)$, provides the asymmetry which is seen in the original. The transverse shape of $\mathbf{p}^{(2)}$ shows that the laser stripe on the right side has its maximum just at the time when the left one assumes its smallest intensity values, and vice versa. The second eigenvector $\mathbf{p}^{(2)}$ thus describes the broken symmetry between the two laser stripes. Generally, the magnitude of $\lambda^{(\alpha)} = \langle (\mathbf{p}^{(\alpha)}, u)^2 \rangle_t$ is an indication for the content of $\mathbf{p}^{(\alpha)}$ in the spatiotemporal pattern analyzed. Consequently, as one would expect from simple comparison of the corresponding Figs. 3 (b) and 3 (a), $\lambda^{(2)} = 0.4001$ shows that the second eigenmode significantly contributes to the original [Fig. 3 (a)]. The projection of the spatiotemporal data onto the coupling mode $p^{(3)}$ [Fig. 3 (d)], where the intensity distribution between the two stripes is enhanced, visualizes the otherwise concealed irregular intensity flares which couple the two stripes with each other. Changing in space and time, these intensity tongues, which characterize the exchange of energy between the two stripes, indicate that the interelement coupling mechanism itself is not constant. It changes both in space and in time. The transverse shape of $\mathbf{p}^{(4)}$ and $\mathbf{p}^{(5)}$ and the projected intensity distributions indicate that each laser stripe can dynamically support — next to the single cw transverse mode — to a certain degree two or even three transverse modes (bimodal mode, trimodal mode). In the case of the strongly coupled twin-stripe laser (Fig. 4), the synchronizing fundamental mode $p^{(1)}$, which now also contributes significantly to the intensity coupling between the laser stripes, and the symmetry-breaking mode $\mathbf{p}^{(2)}$ are the most dominant in the spatiotemporal intensity distribution. High-frequency out-of-phase oscillation of the two laser stripes is confirmed: Clearly $\mathbf{p}^{(2)}$ is vital to describe the phase lag between the laser stripes which causes the typical oscillations observed in the original [Fig. 4 (a)]. The bimodal mode [Fig. 4 (d)] and the coupling mode [Fig. 4 (e)] also contribute slightly, while the

higher modes [Fig. 4 (f)] represent negligible noise. If an accuracy of 10^{-4} in $\sum_{\alpha} \lambda^{(\alpha)}$ is required, only the first three modes are necessary, as compared to five modes in Fig. 3. Thus the number of active eigenmodes, i.e., spatiotemporal degrees of freedom, is reduced as compared to the intermediate-coupling regime (Fig. 3). This reflects the stronger spatial coherence and explains the more regular dynamics in the case of $s=5~\mu\mathrm{m}$.

With the paradigm of the twin-stripe semiconductor laser it has thus been demonstrated that the singular spectrum analysis is a powerful tool for the investigation of spatially distributed nonlinear dynamic systems. Experiments on commercially available ten-stripe lasers [15] show qualitatively similar behavior. The symmetry breaking mode, the coupling mode, and the bimodal mode are clearly identified next to the synchronizing fundamental mode. These modes, although generally not noticeably in common shadow plots due to the affluence of information from the spatiotemporal intensity distributions, do significantly determine the dynamics of the coupled laser oscillators. In particular, the interelement coupling between the two oscillators itself changes in space and time. Consequently, assuming a spatially and temporally constant coupling parameter for describing the evanescent coupling between the two laser oscillators [2], will not adequately cover all the relevant spatiotemporal dynamics. To demonstrate the wider applicability of our approach, we have applied our method to the investigation of electrical instabilities and current filamentation in semiconductor transport [16] and found similar fundamental eigenmodes [17]. Moreover, we propose that our approach also applies to the interpretation of spatiotemporal patterns in nonlinear optics of liquid crystals [18]. Thus a deeper understanding may be gained of the processes which involve the combination of spatial and temporal degrees of freedom, in the laminar regime as well as in the regime of spatiotemporal complexity and chaos.

We thank H.-P. Herzel, R. Döttling, G. Hüpper, A. Wacker, and, in particular, K. Krischer for valuable and interesting discussions. Partial financial support from the Deutsche Forschungsgemeinschaft is gratefully acknowledged.

^[1] N. B. Abraham and W. J. Firth, J. Opt. Soc. Am. B 7, 951 (1990).

 ^[2] S. S. Wang and H. G. Winful, Appl. Phys. Lett. 52, 1774 (1988); H. G. Winful and L. Rahman, Phys. Rev. Lett. 65, 1575 (1990).

^[3] K. Otsuka, Phys. Rev. Lett. 65, 329 (1990).

^[4] L. Rahman and H. G. Winful, Nonlinear Dynamics in Optical Systems 1992 Technical Digest Series (Optical Society of America, Washington, D.C., 1992), Vol. 16, Abstract ThB3-1.

^[5] H. Adachihara, O. Hess, R. Indik, and J. V. Moloney, J. Opt. Soc. Am. B 10, 496 (1993).

 ^[6] O. Hess, Spatio-Temporal Dynamics of Semiconductor Lasers (Wissenschaft und Technik Verlag, Berlin, 1993);
 O. Hess and E. Schöll, Physica (Amsterdam) D 70, 165

^{(1994).}

^[7] G. P. Agrawal and N. K. Dutta, Long-Wavelength Semiconductor Lasers (Van Nostrand Reinhold, New York, 1986).

^[8] M. Lax, W. H. Louisell, and W. B McKnight, Phys. Rev. A 11, 1365 (1975).

^[9] K. Tai, T. R. Hayes, S. L. McCall, and W. T. Tsang, Appl. Phys. Lett. 53, 302 (1988).

^[10] I. S. Grieg and J. D. Morris, J. Comp. Phys. 20, 60 (1976).

^[11] R. K. DeFreez, D. J. Bossert, N. Yu, K. Harnett, R. A. Elliott, and H. G. Winful, Appl. Phys. Lett. 53, 2380 (1988); N. Yu, R. K. DeFreez, D. J. Bossert, R. A. Elliott, H. G. Winful, and D. F. Welsh, Electron. Lett. 24, 1203 (1988).

- [12] L. Sirovich, Quart. Appl. Math. XLV, 561 (1987).
- [13] R. Vautard and M. Ghil, Physica (Amsterdam) D 35, 395 (1989).
- [14] A. E. Deane, I. G. Kevrekidis, G. E. Karniadakis, and S. A. Orszag, Phys. Fluids A 3, 2337 (1991).
- [15] R. A. Elliott, R. K. DeFreez, T. L. Paoli, R. D. Burnham, and W. Streifer, IEEE J. Quant. Electron. QE-21, 598

(1985).

- [16] G. Hüpper, K. Pyragas, and E. Schöll, Phys. Rev. B 48, 17633 (1993).
- [17] O. Hess and E. Schöll (unpublished).
- [18] R. Macdonald and H. J. Eichler, Opt. Commun. 89, 289 (1992); M. Kreuzer, H. Gottschling, and T. Tschudi, Mol. Cryst. Liq. Cryst. 198, 231 (1991).

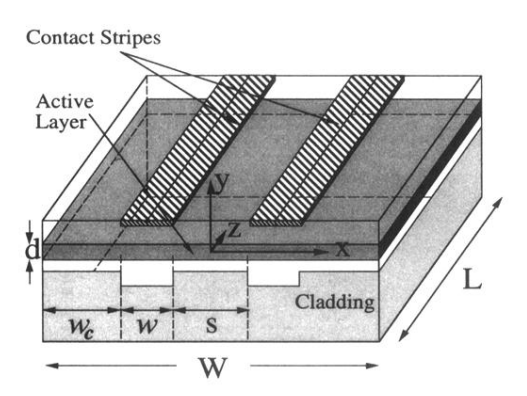


FIG. 1. Schematic structure of a combined gain- and index-guided ${\rm GaAs/Al_zGa_{1-x}As}$ twin-stripe laser.

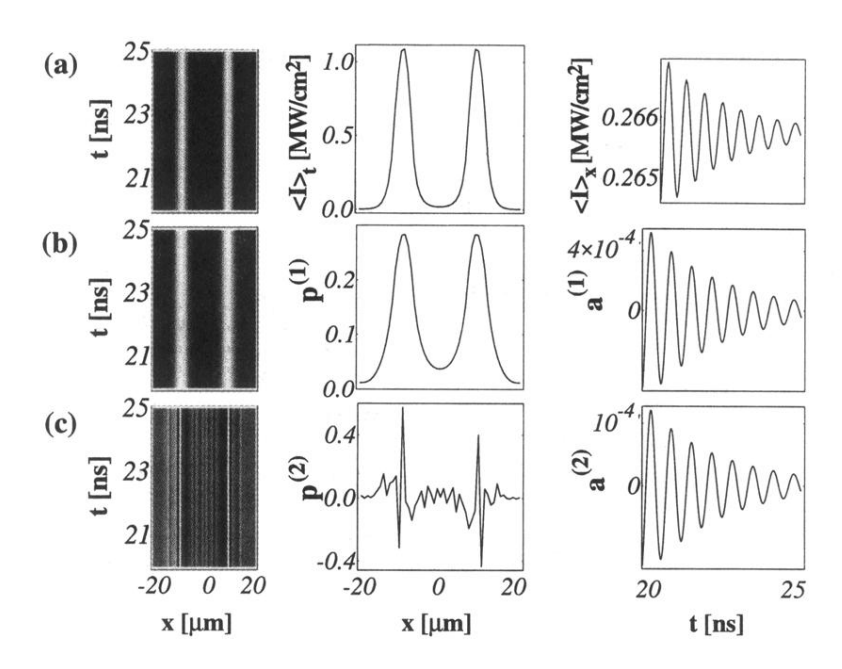


FIG. 2. Computed near-field intensity I(x,t) for the weakly coupled twin-stripe semiconductor laser at a stripe separation of $s=14~\mu\mathrm{m}$. (a) Original spatiotemporal intensity distribution (Bright colors represent high light intensity, dark shading indicates low intensity values); temporally averaged intensity $\langle I \rangle_t$; transverse spatial average $\langle I \rangle_x$. (b) Reconstructed spatiotemporal intensity distribution, eigenvector $\mathbf{p}^{(1)}$, and expansion coefficient $a^{(1)}$, obtained by projection onto the fundamental eigenmode $(\lambda^{(1)}=0.9983)$. (c) Projection onto the second eigenmode $(\lambda^{(2)}<10^{-3})$. The analysis is done for M=51. Only in the reconstructed intensity distribution of the first mode $\langle I \rangle_t$ has been added.

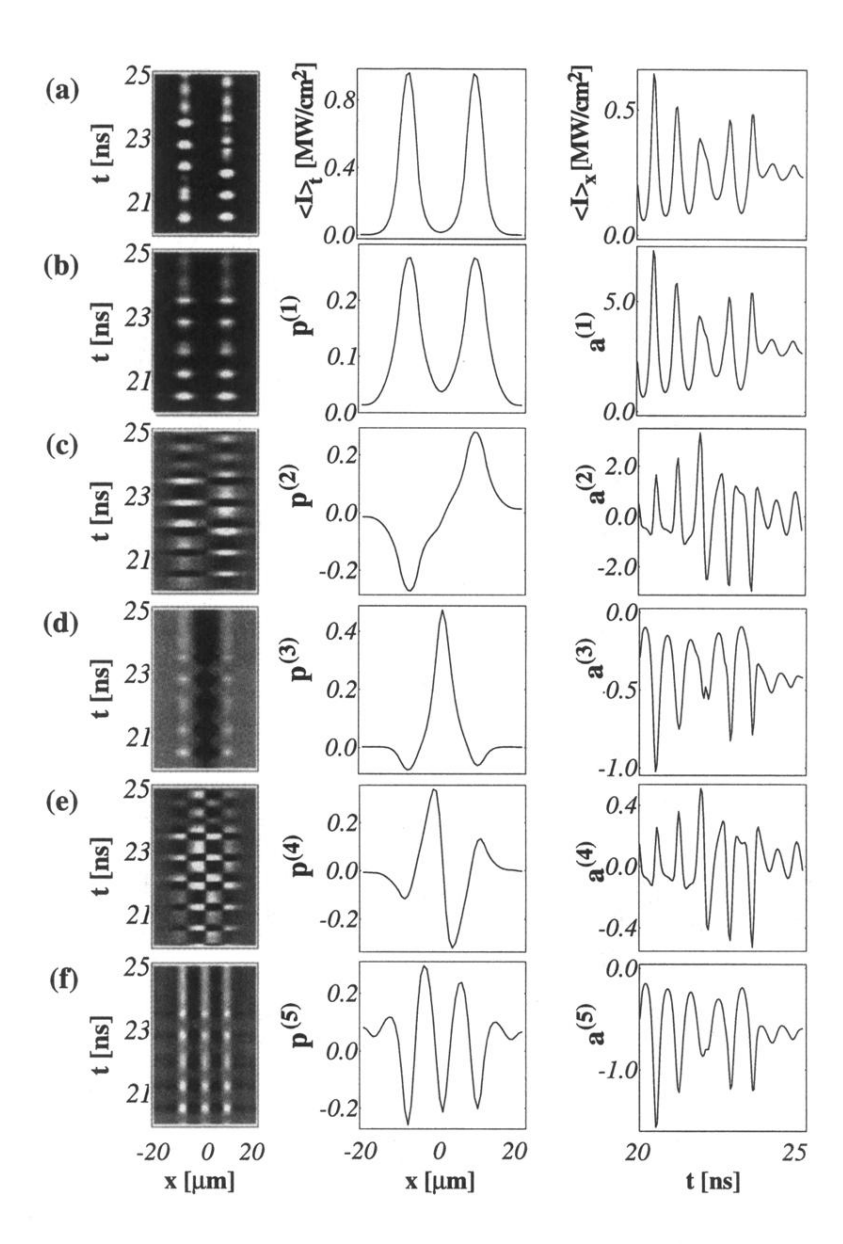


FIG. 3. Intermediate coupling regime (s = 12 μ m). (a) Original, (b) – (f) reconstructed spatiotemporal intensity distribution, obtained by projection onto the fundamental mode ($\lambda^{(1)}=0.5822$) (b), the symmetry-breaking mode ($\lambda^{(2)}=0.4001$) (c), the coupling mode ($\lambda^{(3)}=1.412\times 10^{-2}$) (d), and the bimodal ($\lambda^{(4)}=2.935\times 10^{-3}$) (e) and trimodal modes ($\lambda^{(5)}=1.58\times 10^{-4}$) (f).

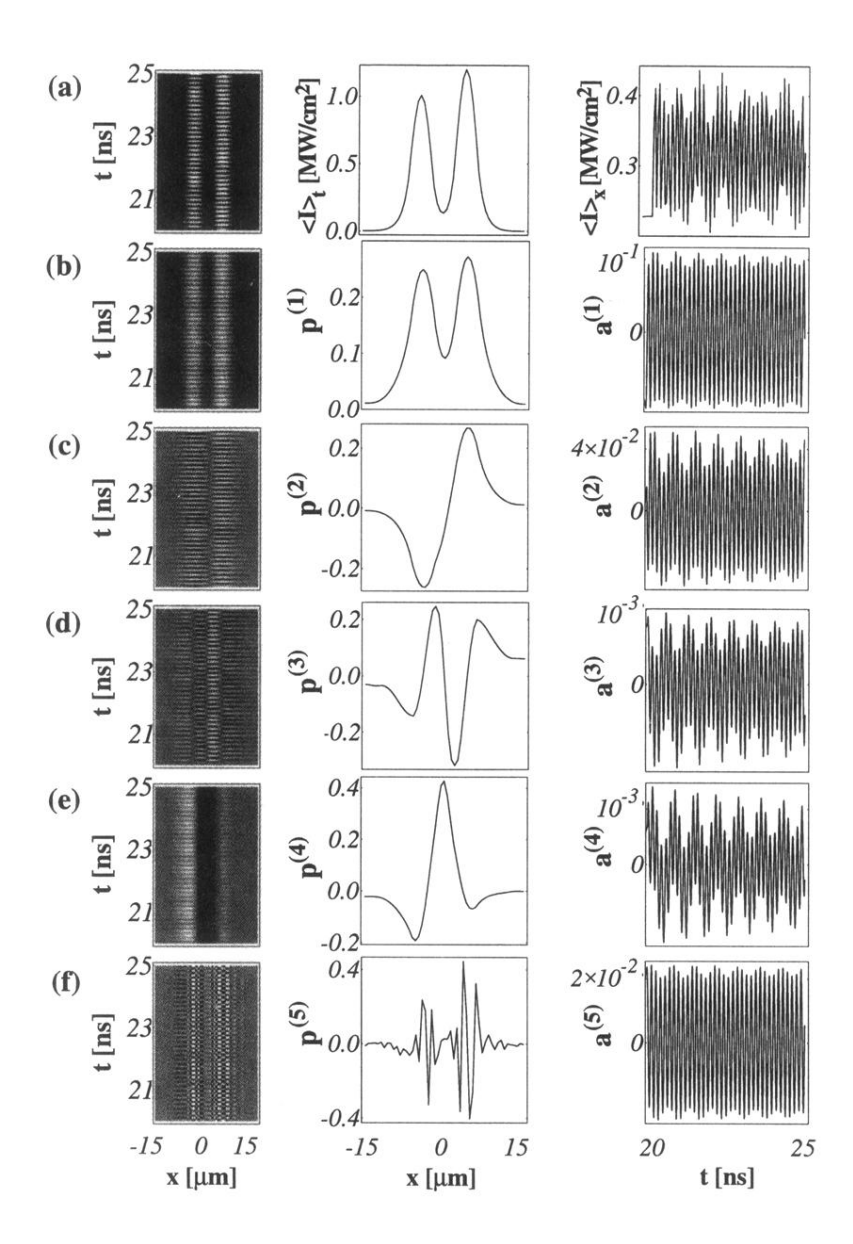


FIG. 4. Same as Fig. 3, but for the strong-coupling regime $(s=5~\mu\mathrm{m})$. (b) $\lambda^{(1)}=0.8534$, (c) $\lambda^{(2)}=0.1459$, (d) $\lambda^{(3)}=6.7\times10^{-4}$, (e) $\lambda^{(4)}=1.19\times10^{-6}$, (f) $\lambda^{(5)}=2.27\times10^{-7}$.